NANO LETTERS

pubs.acs.org/NanoLett Letter

Optical Imaging of Ultrafast Phonon-Polariton Propagation through an Excitonic Sensor

Shan-Wen Cheng, Ding Xu, Haowen Su, James M. Baxter, Luke N. Holtzman, Kenji Watanabe, Takashi Taniguchi, James C. Hone, Katayun Barmak, and Milan Delor*

Cite This: *Nano Lett.* 2023, 23, 9936−9942 Read Online

ACCESS | Metrics & More | Article Recommendations | Supporting Information

ABSTRACT: Hexagonal boron nitride (hBN) hosts phonon polaritons (PhP), hybrid light−matter states that facilitate electromagnetic field confinement and exhibit long-range ballistic transport. Extracting the spatiotemporal dynamics of PhPs usually requires "tour de force" experimental methods such as ultrafast near-field infrared microscopy. Here, we leverage the remarkable environmental sensitivity of excitons in two-dimensional transition metal dichalcogenides to image PhP propagation in adjacent hBN slabs. Using ultrafast optical microscopy on monolayer WSe_2/hBN heterostructures, we image propagating PhPs from 3.5 K to room temperature with subpicosecond and few-nanometer precision. Excitons in WSe_2 act as transducers between visible light pulses and infrared PhPs, enabling visible-light imaging of PhP transport with far-field microscopy. We also report evidence of excitons in WSe_2 copropagating with hBN PhPs over several micrometers. Our results provide new avenues for imaging polar excitations over a large frequency range with extreme spatiotemporal precision and new mechanisms to realize ballistic exciton transport at room temperature.

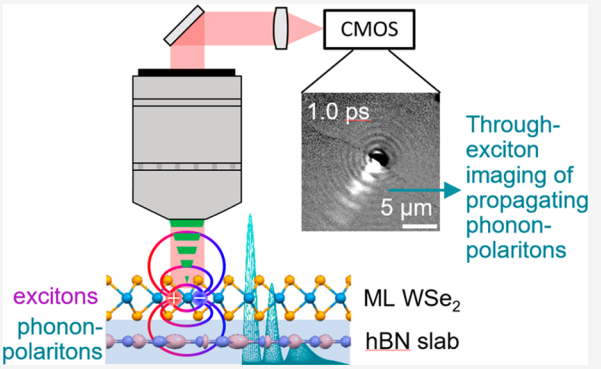

KEYWORDS: *hyperbolic phonon-polaritons, hexagonal boron nitride, exciton sensor, ultrafast microscopy, van der Waals heterostructure, polariton transport*

When light hybridizes with collective oscillations of polar excitations, new particles known as polaritons form.[1−4] Polaritons in van der Waals (vdW) materials have attracted great interest as platforms to confine light at the nanoscale, dramatically enhancing light-matter interactions and enabling the transport of energy and information at light-like speeds in deeply subwavelength structures.[2,5−10] Hyperbolic phonon-polaritons (PhPs) in thin hexagonal boron nitride (hBN) slabs are collective optical phonons coupled to photons that confine mid-infrared light to sub-100 nm dimensions, enabling subdiffraction imaging and strong interactions with local dipoles.[2,11−16] PhPs in hBN also exhibit remarkably long (picosecond) lifetimes and micrometer-scale propagation lengths even in the presence of compositional heterogeneity, thus holding great promise as information carriers in nanophotonic structures.[8,11,17,18]

Few approaches are capable of probing the spatiotemporal dynamics of PhPs in vdW materials. High spatiotemporal resolution and the ability to overcome the momentum mismatch between free-space photons and polaritons are prerequisites for imaging these confined PhPs.[2] The most widespread and impactful approach to-date is infrared scattering-type scanning near-field optical microscopy (SNOM).[8,11,13,19−21] Time-domain interferometric SNOM realizations have enabled spatiotemporal imaging of PhP propagation in hBN slabs, revealing picosecond lifetimes and propagation over several micrometers,[17] in agreement with lifetimes indirectly inferred from steady-state measurements.[16,22−26] Recently, PhPs were also resolved using ultrafast electron microscopy, revealing complex spatiotemporal dynamics including wavepacket acceleration, deceleration, and splitting.[18] While powerful, these approaches may be difficult to implement in more complex heterostructures, in particular to spatiotemporally resolve interactions between PhPs and other species such as molecules, electrons, and excitons in adjacent or buried layers. Here, we adopt a fundamentally different approach to image PhP propagation: we leverage excitons in an adjacent monolayer semiconductor as sensors that transduce PhPs into an optically readable signal, which we monitor in the far-field through ultrafast visible-to-near-IR microscopy to track PhP propagation in hBN slabs (Figure 1a).

Received: August 1, 2023
Revised: October 11, 2023
Published: October 18, 2023

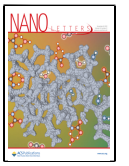

https://doi.org/10.1021/acs.nanolett.3c02897
Nano Lett. 2023, 23, 9936−9942

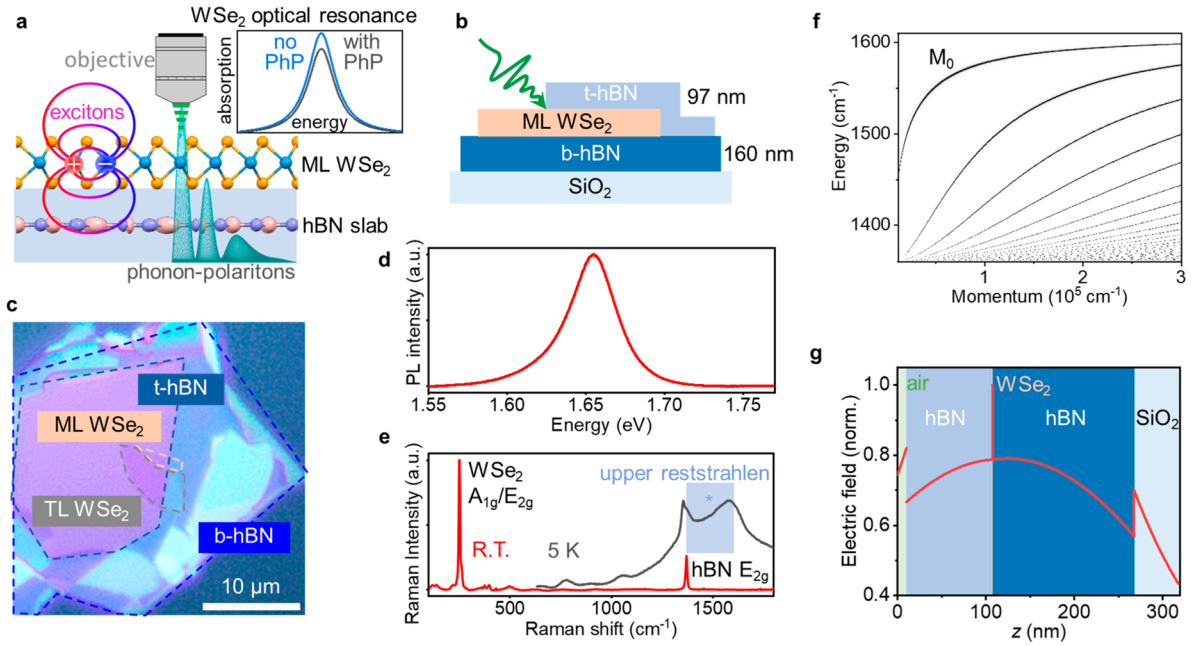

Figure 1. Excitons and PhPs in vdW heterostructures. (a) Schematic of PhP sensing with ML semiconductor excitons in a WSe_2/hBN heterostructure. PhPs modify the local WSe_2 exciton polarizability, thus modulating the excitonic resonance, which can be optically monitored in the far-field. (b) Illustration of the heterostructure labeled sample 1 in the text. (c) Optical microscope image of the heterostructure. Different layers are enclosed by dashed lines. (d) PL spectrum of the encapsulated ML WSe_2 at room temperature. (e) Raman spectra of the hBN/WSe_2/hBN heterostructure at room temperature (red) and 5 K (gray). A band in the upper reststrahlen region (indicated with a blue rectangle) appears in the heterostructure at 5 K upon above-gap excitation of WSe_2 in the heterostructure. More details are provided in Figure S3. (f) Calculated PhP dispersion in the upper reststrahlen band for the stack plotted in panel (b). (g) Calculated in-plane electric field distribution of the M_0 PhP mode as a function of the depth of the stack. The field strength is plotted for a momentum of 10^5 cm^{-1}.

As a sensor layer, we use monolayer (ML) WSe_2, an archetypal two-dimensional transitional metal dichalcogenide (2D TMD) semiconductor.[27−31] Weak out-of-plane dielectric screening in ML TMDs results in strongly bound electron−hole pairs (excitons) even at room temperature.[32−35] Since exciton field lines extend beyond the ML plane,[33] the exciton binding energy and oscillator strength are highly sensitive to perturbations in the dielectric environment, which modify electron−hole interactions.[29,33,36,37] This extreme sensitivity has been exploited to characterize dielectric disorder in surrounding media and to funnel excitons with nanometric precision.[37−39] Remarkably, although excitons exhibit a resonance at optical frequencies, they can sense environmental perturbations that occur over a large frequency range, including correlated electronic states with characteristic responses in the GHz-THz range.[40] Furthermore, recent experiments have shown that interfacial coupling between excitons in TMDs and phonons in hBN can be strong,[41−44] notably enabling the generation of mid-infrared PhPs in hBN through visible light excitation of adjacent TMD monolayers via resonant Raman scattering.[43] Herein, we leverage the broad-bandwidth sensitivity of excitons to dielectric perturbations to track PhP propagation using ultrafast optical microscopy in ML WSe_2/hBN heterostructures (Figure 1a). These measurements enable direct extraction of PhP propagation velocity and lifetime, albeit without momentum selectivity. Importantly, our results also provide new insight into interfacial exciton−PhP interactions; we notably report evidence of PhP-assisted exciton flow, suggesting strong interlayer exciton−PhP coupling, and a novel method to transport electronic energy with minimal scattering at light-like speeds in vdW heterostructures.

We create hBN/ML-WSe_2/hBN heterostructures as depicted in Figure 1b, using mechanical exfoliation and a dry-stamping flip-chip approach (Supplementary Section 1). We expose an hBN edge in the middle of the WSe_2 to facilitate the generation of hBN PhPs with large in-plane momentum upon excitation.[2,18] An optical image of the structure is shown in Figure 1c. The room-temperature photoluminescence (Figure 1d) spectrum in the encapsulated region shows the characteristic A-exciton peak of ML WSe_2 at 1.654 eV. The room-temperature Raman spectrum (Figure 1e) displays the ∼250 cm^{-1} near-degenerate A_{1g} and E_{2g} modes of WSe_2 and the 1369 cm^{-1} E_{2g} mode in hBN. Both spectra are in close agreement with previously reported values.[43,45−48] At cryogenic temperatures, we observe the emergence of new hBN Raman modes in the heterostructure upon above-gap excitation of WSe_2. Specifically, an intense new resonant Raman band at frequencies associated with the upper reststrahlen band of hBN (Figures 1e and S3) appears following 532 nm excitation. This band is only visible in the WSe_2/hBN heterostructure and is absent in hBN-only regions (Figure S3), indicating strong interlayer exciton−phonon interactions and resonance-assisted excitation of PhPs. Recent studies[43] also show such hybrid bands associated with hyperbolic hBN PhPs upon resonant excitation of WSe_2 in heterostructures, though primarily focus on the emergence of bands associated with the lower reststrahlen band. Figure 1f shows the calculated energy-momentum dispersion relation for the full stack of Figure 1b in the frequency region of the upper reststrahlen band, confirming the presence of multiple PhP branches. The field distribution of the fundamental M_0 mode is plotted in Figure 1g;[49] the presence of the WSe_2 minimally perturbs the field distribution in the hBN, suggesting it acts as

https://doi.org/10.1021/acs.nanolett.3c02897
Nano Lett. 2023, 23, 9936−9942

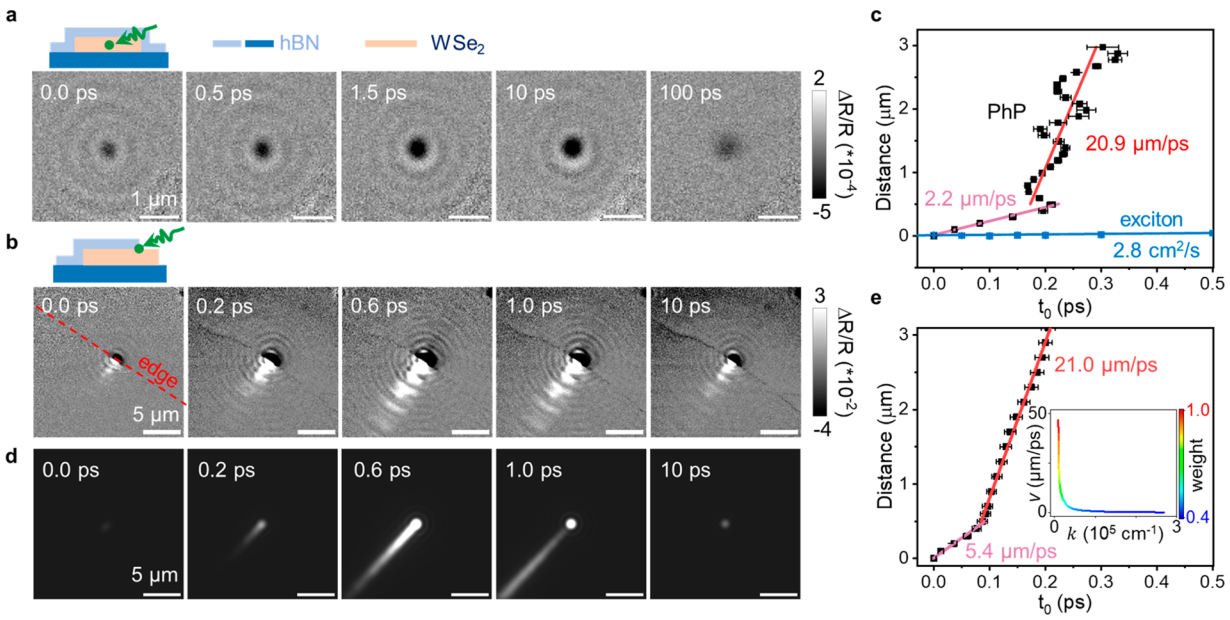

Figure 2. Imaging exciton and PhP propagation with far-field ultrafast optical microscopy. (a) stroboSCAT pump−probe images in a hBN-encapsulated ML WSe_2 control structure, displaying pure exciton transport. (b) stroboSCAT pump−probe images with the pump beam focused on the edge of the top-layer hBN. The red dashed line in the first frame denotes the top hBN edge. The pump is at 2.40 eV, and the probe is at 1.67 eV. (c) Propagation analysis for excitons from panel (a) and PhPs from panel (b). The oscillations observed in the PhP propagation analysis are experimental artifacts caused by the presence of strong diffraction rings evident in panel b (Figure S10). (d) Monte Carlo simulations of exciton and PhP transport. The PhP velocity is modeled according to the calculated dispersion of the M_0 mode of Figure 1f, as shown in the inset of panel (e). (e) Propagation analysis of the Monte Carlo simulations from panel (d). Inset: group velocity distribution used to simulate the PhP wavepacket. The color bar represents the population weight. Error bars are all one standard deviation. All data and simulations are at room temperature.

a sensor inserted in the middle of the hBN slab. Dispersion and field distribution calculations for a stack of different thicknesses (Figure S4) that we also investigated are shown in Figure S5.

To image PhP propagation with high spatiotemporal resolution, we use stroboscopic scattering microscopy (stroboSCAT, Supplementary Section 2), a spatiotemporally resolved ultrafast optical imaging approach based on interferometric scattering[50−52] that affords femtosecond temporal resolution and few-nanometer sensitivity to spatial motion.[53−55] A diffraction-limited visible pump pulse generates a localized population of excitons in the TMD, and of PhPs in hBN. At controllable time delays later, a widefield back-scattering probe pulse preresonant with the WSe_2 A-exciton images the sample with and without the pump pulse. Varying the pump−probe time delay allows building movies of species propagation over femtoseconds−nanoseconds and nanometers−micrometers. Although there are many processes through which optical excitation can excite low-frequency PhPs,[43,56−62] the Raman spectra displayed in Figures 1e and S3 suggest that interlayer exciton−phonon interactions in our heterostructures promote excitation of upper reststrahlen PhPs primarily through a resonant Raman process. We further posit that the presence of pump-generated PhPs in hBN locally modifies the dielectric function of the heterostructure. Since the A-exciton optical resonance of WSe_2 is highly sensitive to tiny changes in local dielectric, the presence of PhPs in hBN is associated with a change in the oscillator strength and/or shift of the WSe_2 optical resonance (Figure 1a). Our preresonant stroboSCAT probe[38] reports directly on this PhP-induced change in the WSe_2 resonance, thus mapping the spatial distribution of propagating PhPs at any given time after excitation.

stroboSCAT images following the excitation of hBN/WSe_2/hBN heterostructures are shown in Figure 2. When exciting away from any hBN edge in a control structure (Figure 2a), we observe pump-generated excitons in WSe_2 exhibiting normal diffusive transport at 2.8 ± 0.2 cm^2/s, in reasonable agreement with the literature.[63−65] Note that the sign of the contrast in these measurements depends on the hBN thickness due to interference effects (Figure S7). Our key result is that we observe strikingly different behavior when exciting at the hBN edge of our heterostructure (Figure 2b). Aside from the central circular signal corresponding to WSe_2 excitons, we observe a bright signal that rapidly propagates into the hBN/WSe_2/hBN region, perpendicularly to the hBN edge and over several micrometers in less than a picosecond. This optical signal arises from a change in the WSe_2 polarizability at our probe wavelength of 1.67 eV due to the WSe_2's response to a propagating species. The spatial evolution of the propagating signal is analyzed in Figure 2c by monitoring the wavefront arrival time at different distances from the excitation spot (Supplementary Section 5),[66] displaying two characteristic velocities of 2.2 ± 0.1 μm/ps and 20.9 ± 3.0 μm/ps, i.e., 0.7% and 7% of light speed, with a primary lifetime component of ∼1 ps (lifetimes are analyzed in more detail below). The fact that this propagating signal only appears upon excitation of the hBN edge suggests that the edge acts as a coupler of far-field excitation into species with high in-plane momentum. Indeed flake edges are often used to launch high-momentum PhPs and waveguide modes.[2,18,25] We rule out optical waveguide or surface modes at the excitation wavelength of 2.4 eV since our structure does not support such modes with velocities on the same order of magnitude as those observed (Figure S8).

https://doi.org/10.1021/acs.nanolett.3c02897
Nano Lett. 2023, 23, 9936−9942

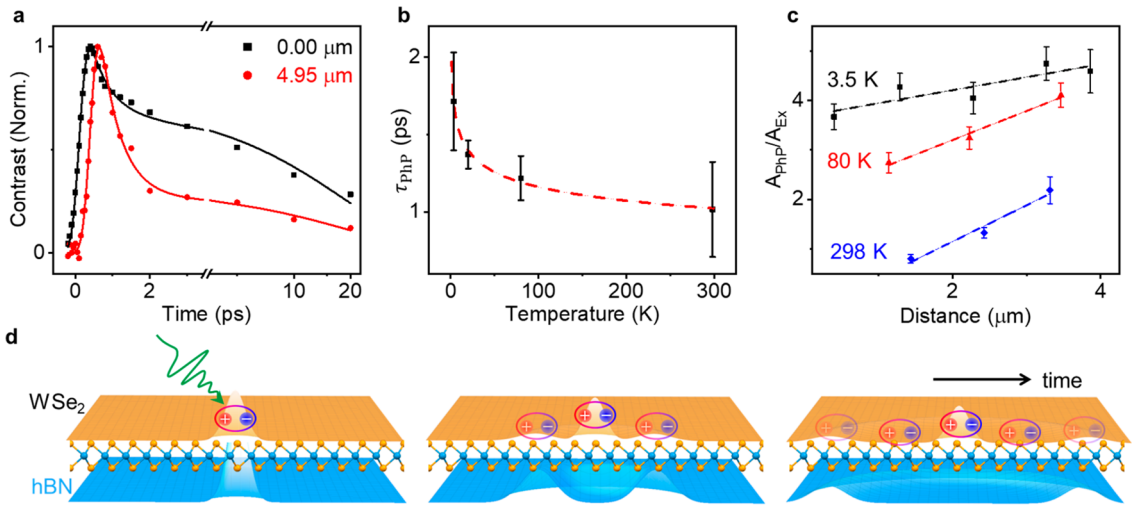

Figure 3. Tracking exciton−PhP interactions. (a) Lin-log plot of reflectance contrast over time delay at different distances from the excitation spot at room temperature, extracted from the data shown in Figure 2b. The lines are biexponential fits. (b) PhP signal lifetime as a function of temperature. The dashed line is a guide to the eye. (c) A_{PhP}/A_{ex} ratio at different distances and temperatures. Dashed lines are guides for the eye. Error bars are all one standard deviation. (d) Schematic of PhP-assisted exciton transport in ML WSe_2/hBN heterostructures.

Instead, the observed propagation speed corresponds closely to that expected for hBN PhPs in the investigated slabs, as shown by Monte Carlo simulations in Figure 2d,e. In these simulations, we include a slowly diffusing population of excitons at the excitation spot and a population of PhPs excited by the pump pulse that propagate ballistically at a group velocity determined by the calculated dispersion of Figure 1f. We only consider the zeroth-order mode (TM_0),[67,68] for which the density of polaritonic states is expected to be largest,[17,18] and populate this mode according to a Maxwell−Boltzmann distribution (Figure 2e inset, simulation details in Supplementary Section 6). Images generated from these simulations are shown in Figure 2d. Figure 2e plots the simulated propagation by using the same analysis as that used in Figure 2c. The turnover and extracted velocities of 5.4 ± 0.3 μm/ps and 21.0 ± 0.5 μm/ps are in reasonable agreement with the experimental data. The turnover from slow to fast propagation is a result of convolving the exciton signal with the fast-moving wavepacket for early time points, as well as the effect of fitting a single effective velocity to a dispersing wavepacket. The good agreement between experimental and Monte Carlo simulations based on the calculated PhP dispersion for our stack supports our assignment of the fast-propagating signal to hBN PhPs, which are read out optically through WSe_2 in our measurement. Although a systematic hBN thickness-dependent study is outside the scope of this work, we reproduced the propagating signal in stacks with hBN slab thicknesses as low as 33 nm (Figures S4 and S5), suggesting our method is suitable for probing ultraconfined polaritons.

The purpose of pump excitation in the experiments described above is to populate PhPs; however, since excitation above the optical gap of WSe_2 is required to efficiently excite PhPs through resonance enhancement, the pump also inevitably populates excitons in WSe_2. We now turn to characterizing whether interlayer exciton−phonon interactions affect the transport of these pump-generated excitons. Figure 3a displays the signal kinetics at the excitation spot and 4.95 μm away from the excitation region for the data displayed in Figure 2b. At the excitation spot, the signal is dominated by excitons with a lifetime of τ_{ex} = 25 ± 4 ps, in agreement with the literature for encapsulated 2D TMDs.[63,64,69] A few micrometers away, the signal exhibits biexponential decay kinetics, with a first dominating component of τ_{PhP} = 1.1 ± 0.2 ps assigned to hBN PhPs, and a second minor component with a lifetime of 23 ± 5 ps. PhPs in natural-abundance hBN have lifetimes of less than 2 ps,[11,17,21,25] ruling out the assignment of the long-lived component to PhPs. Instead, the correspondence between the decay kinetics of this minor long-lived component and the exciton signal suggests that a finite population of pump-generated excitons has propagated ∼5 μm away from the excitation spot (see the weak leftover bright signal in the 10 ps image of Figure 2b). This finding is surprising: on few-picosecond time scales, we do not expect any exciton propagation beyond a micrometer (Figure 2a,c). Since this exciton signal follows the propagation direction and speed of PhPs, our observations indicate that a small fraction of pump-generated excitons copropagate with PhPs. We postulate that PhPs in hBN couple to excitons in WSe_2 through a deformation potential-type interaction, similar to studies exploring the use of surface acoustic waves in piezoelectric slabs to transport excitons in adjacent TMDs or III−V semiconductors.[70−74] The key difference, however, is that PhPs propagate 3 orders of magnitude faster than acoustic waves. Thus, the mechanism we unveil here enables electronic energy to be transported ballistically at a substantial fraction of the speed of light through interfacial exciton−PhP coupling in van der Waals heterostructures.

To lend further support to our hypotheses, we carried out temperature-dependent measurements of the PhP and exciton signals (Figure 3b,c). First, at cryogenic temperatures, PhPs should exhibit longer lifetimes due to fewer damping pathways. Indeed, we find that τ_{PhP} increases almost 2-fold at 3.5 K compared to room temperature (Figure 3b). Both the temperature trend and absolute lifetimes concur with literature reports,[11,47] providing further confidence that the propagating signal can be associated primarily with hBN PhPs. Next, to better understand the nature of exciton−PhP coupling, we studied the contributions of PhPs and excitons to the signal contrast as a function of the distance at different temperatures

https://doi.org/10.1021/acs.nanolett.3c02897
Nano Lett. 2023, 23, 9936−9942

(Figure 3c). Since the signals associated with PhPs and excitons stem from the same excitonic optical response, we use the ratio A_{PhP}/A_{ex}, where A corresponds to the respective amplitudes of the biexponential fit, as an estimate of the PhP/exciton population ratio for a given temperature. As shown in Figure 3c, for increasing distances from the excitation, the PhP/exciton ratio increases. This observation indicates that excitons do not copropagate with PhPs over the whole distance (Figure 3d): excitons scatter out of the copropagating state faster than PhP damping. At 3.5 K, the distance dependence is suppressed, suggesting that excitons copropagate with PhPs over longer distances compared to room temperature. These observations are consistent with an interfacial exciton−PhP interaction that leads to a weakly bound state; the latter can be destroyed by thermal fluctuations, again in close analogy to exciton transport mediated by surface acoustic waves.[70−74]

Overall, our results reveal two new concepts of fundamental importance for studying polaritons and realizing novel transport phenomena in vdW materials. First, we show that the exciton resonance at optical frequencies in TMD monolayers can act as a sensor of propagating mid-IR PhPs in adjacent hBN slabs. We leverage this novel concept to image PhP propagation in WSe_2/hBN heterostructures with femtosecond resolution and nanometer−micrometer spatial dynamic range using visible-light far-field ultrafast scattering microscopy. The ease of our approach compared to the current state-of-the-art,[8,18] however, comes at an expense, since it does not allow momentum- and energy-selective excitation of PhPs. Future experiments using resonant mid-IR excitation of PhPs and through-TMD visible-light imaging will provide energy and momentum selectivity while retaining the high spatiotemporal resolution and ease of our approach, and will enable testing the momentum dependence of our proposed exciton sensing mechanism. Future studies will also expand to tracking the spatiotemporal evolution of other fascinating excitations in vdW materials, including THz polaritons, magnons, and correlated states. Second, we have shown that excitons are not just passive observers of PhPs in these van der Waals heterostructures: strong interlayer exciton−phonon interactions allow PhPs to carry excitons over finite distances (Figure 3d). This coupled motion enables excitons to move ballistically over several micrometers in picoseconds, multiple orders of magnitude faster than through normal exciton diffusion. These results pave a new path for the ultrafast, subdiffraction transport of electronic energy and information in vdW heterostructures.

■ ASSOCIATED CONTENT

Supporting Information

The Supporting Information is available free of charge at https://pubs.acs.org/doi/10.1021/acs.nanolett.3c02897.

Heterostructure fabrication and characterization (Figures S1−S5), Optical instrumentation (Figure S6), additional stroboSCAT data and analysis (Figures S7−S10), details of Monte Carlo simulations (Figure S11) (PDF)

■ AUTHOR INFORMATION

Corresponding Author

Milan Delor − *Department of Chemistry, Columbia University, New York, New York 10027, United States;* orcid.org/0000-0002-9480-9235; Email: milan.delor@columbia.edu

Authors

Shan-Wen Cheng − *Department of Chemistry, Columbia University, New York, New York 10027, United States*

Ding Xu − *Department of Chemistry, Columbia University, New York, New York 10027, United States*

Haowen Su − *Department of Chemistry, Columbia University, New York, New York 10027, United States;* orcid.org/0000-0002-8402-4258

James M. Baxter − *Department of Chemistry, Columbia University, New York, New York 10027, United States;* orcid.org/0000-0002-4641-6760

Luke N. Holtzman − *Department of Applied Physics and Applied Mathematics, Columbia University, New York, New York 10027, United States*

Kenji Watanabe − *Research Center for Electronic and Optical Materials, National Institute for Materials Science, Tsukuba 305-0044, Japan;* orcid.org/0000-0003-3701-8119

Takashi Taniguchi − *Research Center for Materials Nanoarchitectonics, National Institute for Materials Science, Tsukuba 305-0044, Japan;* orcid.org/0000-0002-1467-3105

James C. Hone − *Department of Mechanical Engineering, Columbia University, New York, New York 10027, United States;* orcid.org/0000-0002-8084-3301

Katayun Barmak − *Department of Applied Physics and Applied Mathematics, Columbia University, New York, New York 10027, United States*

Complete contact information is available at: https://pubs.acs.org/10.1021/acs.nanolett.3c02897

Notes

The authors declare no competing financial interest.

■ ACKNOWLEDGMENTS

We thank Prof. Dmitri Basov (Columbia) for helpful discussions. Research on phonon-polaritons is supported as part of Programmable Quantum Materials, an Energy Frontier Research Center funded by the US Department of Energy (DOE), Office of Science, Basic Energy Sciences (BES), under award DE-SC0019443. Instrument development and sample characterization was supported by the NSF under grant number DMR-2115625 (M.D.). M.D. acknowledges support from the Arnold and Mabel Beckman Foundation through a Beckman Young Investigator award. Synthesis of WSe_2 (L.H., K.B. & J.H.) was supported by the NSF MRSEC program at Columbia through the Center for Precision-Assembled Quantum Materials (DMR-2011738). K.W. and T.T. acknowledge support from the JSPS KAKENHI (Grant Numbers 21H05233 and 23H02052) and World Premier International Research Center Initiative (WPI), MEXT, Japan.

■ REFERENCES

(1) Ritchie, R. H. Plasma Losses by Fast Electrons in Thin Films. *Phys. Rev.* **1957**, *106*, 874−881.

(2) Basov, D. N.; Fogler, M. M.; García de Abajo, F. J. Polaritons in van Der Waals Materials. *Science* **2016**, *354*, aag1992.

(3) Hopfield, J. J. Theory of the Contribution of Excitons to the Complex Dielectric Constant of Crystals. *Phys. Rev.* **1958**, *112*, 1555−1567.

(4) Mills, D. L.; Burstein, E. Polaritons: The Electromagnetic Modes of Media. *Rep. Prog. Phys.* **1974**, *37*, 817−926.
(5) Basov, D. N.; Asenjo-Garcia, A.; Schuck, P. J.; Zhu, X.; Rubio, A. Polariton Panorama. *Nanophotonics* **2020**, *10*, 549−577.
(6) Low, T.; Chaves, A.; Caldwell, J. D.; Kumar, A.; Fang, N. X.; Avouris, P.; Heinz, T. F.; Guinea, F.; Martin-Moreno, L.; Koppens, F. Polaritons in Layered Two-Dimensional Materials. *Nat. Mater.* **2017**, *16*, 182−194.
(7) Basov, D. N.; Averitt, R. D.; Hsieh, D. Towards Properties on Demand in Quantum Materials. *Nat. Mater.* **2017**, *16*, 1077−1088.
(8) Dai, S.; Fei, Z.; Ma, Q.; Rodin, A. S.; Wagner, M.; McLeod, A. S.; Liu, M. K.; Gannett, W.; Regan, W.; Watanabe, K.; Taniguchi, T.; Thiemens, M.; Dominguez, G.; Neto, A. H. C.; Zettl, A.; Keilmann, F.; Jarillo-Herrero, P.; Fogler, M. M.; Basov, D. N. Tunable Phonon Polaritons in Atomically Thin van Der Waals Crystals of Boron Nitride. *Science* **2014**, *343*, 1125−1129.
(9) Xu, X. G.; Ghamsari, B. G.; Jiang, J.-H.; Gilburd, L.; Andreev, G. O.; Zhi, C.; Bando, Y.; Golberg, D.; Berini, P.; Walker, G. C. One-Dimensional Surface Phonon Polaritons in Boron Nitride Nanotubes. *Nat. Commun.* **2014**, *5*, 4782.
(10) Caldwell, J. D.; Kretinin, A. V.; Chen, Y.; Giannini, V.; Fogler, M. M.; Francescato, Y.; Ellis, C. T.; Tischler, J. G.; Woods, C. R.; Giles, A. J.; Hong, M.; Watanabe, K.; Taniguchi, T.; Maier, S. A.; Novoselov, K. S. Sub-Diffractional Volume-Confined Polaritons in the Natural Hyperbolic Material Hexagonal Boron Nitride. *Nat. Commun.* **2014**, *5*, 5221.
(11) Ni, G.; McLeod, A. S.; Sun, Z.; Matson, J. R.; Lo, C. F. B.; Rhodes, D. A.; Ruta, F. L.; Moore, S. L.; Vitalone, R. A.; Cusco, R.; Artús, L.; Xiong, L.; Dean, C. R.; Hone, J. C.; Millis, A. J.; Fogler, M. M.; Edgar, J. H.; Caldwell, J. D.; Basov, D. N. Long-Lived Phonon Polaritons in Hyperbolic Materials. *Nano Lett.* **2021**, *21*, 5767−5773.
(12) Caldwell, J. D.; Aharonovich, I.; Cassabois, G.; Edgar, J. H.; Gil, B.; Basov, D. N. Photonics with Hexagonal Boron Nitride. *Nat. Rev. Mater.* **2019**, *4*, 552−567.
(13) Dai, S.; Ma, Q.; Andersen, T.; Mcleod, A. S.; Fei, Z.; Liu, M. K.; Wagner, M.; Watanabe, K.; Taniguchi, T.; Thiemens, M.; Keilmann, F.; Jarillo-Herrero, P.; Fogler, M. M.; Basov, D. N. Subdiffractional Focusing and Guiding of Polaritonic Rays in a Natural Hyperbolic Material. *Nat. Commun.* **2015**, *6*, 6963.
(14) Liu, Z.; Lee, H.; Xiong, Y.; Sun, C.; Zhang, X. Far-Field Optical Hyperlens Magnifying Sub-Diffraction-Limited Objects. *Science* **2007**, *315*, 1686−1686.
(15) Argyropoulos, C.; Estakhri, N. M.; Monticone, F.; Alù, A. Negative Refraction, Gain and Nonlinear Effects in Hyperbolic Metamaterials. *Opt. Express* **2013**, *21*, 15037−15047.
(16) Bylinkin, A.; Schnell, M.; Autore, M.; Calavalle, F.; Li, P.; Taboada-Gutièrrez, J.; Liu, S.; Edgar, J. H.; Casanova, F.; Hueso, L. E.; Alonso-Gonzalez, P.; Nikitin, A. Y.; Hillenbrand, R. Real-Space Observation of Vibrational Strong Coupling between Propagating Phonon Polaritons and Organic Molecules. *Nat. Photonics* **2021**, *15*, 197−202.
(17) Yoxall, E.; Schnell, M.; Nikitin, A. Y.; Txoperena, O.; Woessner, A.; Lundeberg, M. B.; Casanova, F.; Hueso, L. E.; Koppens, F. H. L.; Hillenbrand, R. Direct Observation of Ultraslow Hyperbolic Polariton Propagation with Negative Phase Velocity. *Nat. Photonics* **2015**, *9*, 674−678.
(18) Kurman, Y.; Dahan, R.; Sheinfux, H. H.; Wang, K.; Yannai, M.; Adiv, Y.; Reinhardt, O.; Tizei, L. H. G.; Woo, S. Y.; Li, J.; Edgar, J. H.; Kociak, M.; Koppens, F. H. L.; Kaminer, I. Spatiotemporal Imaging of 2D Polariton Wave Packet Dynamics Using Free Electrons. *Science* **2021**, *372*, 1181−1186.
(19) Dai, S.; Ma, Q.; Yang, Y.; Rosenfeld, J.; Goldflam, M. D.; McLeod, A.; Sun, Z.; Andersen, T. I.; Fei, Z.; Liu, M.; Shao, Y.; Watanabe, K.; Taniguchi, T.; Thiemens, M.; Keilmann, F.; Jarillo-Herrero, P.; Fogler, M. M.; Basov, D. N. Efficiency of Launching Highly Confined Polaritons by Infrared Light Incident on a Hyperbolic Material. *Nano Lett.* **2017**, *17*, 5285−5290.
(20) Menabde, S. G.; Boroviks, S.; Ahn, J.; Heiden, J. T.; Watanabe, K.; Taniguchi, T.; Low, T.; Hwang, D. K.; Mortensen, N. A.; Jang, M. S. Near-Field Probing of Image Phonon-Polaritons in Hexagonal Boron Nitride on Gold Crystals. *Sci. Adv.* **2022**, *8*, eabn0627.
(21) Giles, A. J.; Dai, S.; Vurgaftman, I.; Hoffman, T.; Liu, S.; Lindsay, L.; Ellis, C. T.; Assefa, N.; Chatzakis, I.; Reinecke, T. L.; Tischler, J. G.; Fogler, M. M.; Edgar, J. H.; Basov, D. N.; Caldwell, J. D. Ultralow-Loss Polaritons in Isotopically Pure Boron Nitride. *Nat. Mater.* **2018**, *17*, 134−139.
(22) Pavlidis, G.; Schwartz, J. J.; Matson, J.; Folland, T.; Liu, S.; Edgar, J. H.; Caldwell, J. D.; Centrone, A. Experimental Confirmation of Long Hyperbolic Polariton Lifetimes in Monoisotopic (^{10}B) Hexagonal Boron Nitride at Room Temperature. *APL Mater.* **2021**, *9*, 091109.
(23) Ma, W.; Shabbir, B.; Ou, Q.; Dong, Y.; Chen, H.; Li, P.; Zhang, X.; Lu, Y.; Bao, Q. Anisotropic Polaritons in van Der Waals Materials. *InfoMat* **2020**, *2*, 777−790.
(24) Gilburd, L.; Kim, K. S.; Ho, K.; Trajanoski, D.; Maiti, A.; Halverson, D.; de Beer, S.; Walker, G. C. Hexagonal Boron Nitride Self-Launches Hyperbolic Phonon Polaritons. *J. Phys. Chem. Lett.* **2017**, *8*, 2158−2162.
(25) Li, P.; Dolado, I.; Alfaro-Mozaz, F. J.; Nikitin, A. Y.; Casanova, F.; Hueso, L. E.; Vélez, S.; Hillenbrand, R. Optical Nanoimaging of Hyperbolic Surface Polaritons at the Edges of van Der Waals Materials. *Nano Lett.* **2017**, *17*, 228−235.
(26) Duan, J.; Chen, R.; Li, J.; Jin, K.; Sun, Z.; Chen, J. Launching Phonon Polaritons by Natural Boron Nitride Wrinkles with Modifiable Dispersion by Dielectric Environments. *Adv. Mater.* **2017**, *29*, 1702494.
(27) Mueller, T.; Malic, E. Exciton Physics and Device Application of Two-Dimensional Transition Metal Dichalcogenide Semiconductors. *npj 2D Mater. Appl.* **2018**, *2*, 29.
(28) Wang, G.; Chernikov, A.; Glazov, M. M.; Heinz, T. F.; Marie, X.; Amand, T.; Urbaszek, B. Colloquium : Excitons in Atomically Thin Transition Metal Dichalcogenides. *Rev. Mod. Phys.* **2018**, *90*, 021001.
(29) Berkelbach, T. C.; Reichman, D. R. Optical and Excitonic Properties of Atomically Thin Transition-Metal Dichalcogenides. *Annu. Rev. Condens. Matter Phys.* **2018**, *9*, 379−396.
(30) Edelberg, D.; Rhodes, D.; Kerelsky, A.; Kim, B.; Wang, J.; Zangiabadi, A.; Kim, C.; Abhinandan, A.; Ardelean, J.; Scully, M.; Scullion, D.; Embon, L.; Zu, R.; Santos, E. J. G.; Balicas, L.; Marianetti, C.; Barmak, K.; Zhu, X.; Hone, J.; Pasupathy, A. N. Approaching the Intrinsic Limit in Transition Metal Diselenides via Point Defect Control. *Nano Lett.* **2019**, *19*, 4371−4379.
(31) Liu, S.; Liu, Y.; Holtzman, L.; Li, B.; Holbrook, M.; Pack, J.; Taniguchi, T.; Watanabe, K.; Dean, C. R.; Pasupathy, A. N.; Barmak, K.; Rhodes, D. A.; Hone, J. Two-Step Flux Synthesis of Ultrapure Transition-Metal Dichalcogenides. *ACS Nano* **2023**, *17*, 16587−16596.
(32) Zhu, B.; Chen, X.; Cui, X. Exciton Binding Energy of Monolayer WS2. *Sci. Rep.* **2015**, *5*, 9218.
(33) Chernikov, A.; Berkelbach, T. C.; Hill, H. M.; Rigosi, A.; Li, Y.; Aslan, O. B.; Reichman, D. R.; Hybertsen, M. S.; Heinz, T. F. Exciton Binding Energy and Nonhydrogenic Rydberg Series in Monolayer WS_2. *Phys. Rev. Lett.* **2014**, *113*, 076802.
(34) Hanbicki, A. T.; Currie, M.; Kioseoglou, G.; Friedman, A. L.; Jonker, B. T. Measurement of High Exciton Binding Energy in the Monolayer Transition-Metal Dichalcogenides WS_2 and WSe_2. *Solid State Commun.* **2015**, *203*, 16−20.
(35) Berkelbach, T. C.; Hybertsen, M. S.; Reichman, D. R. Theory of Neutral and Charged Excitons in Monolayer Transition Metal Dichalcogenides. *Phys. Rev. B* **2013**, *88*, 045318.
(36) Cho, Y.; Berkelbach, T. C. Environmentally Sensitive Theory of Electronic and Optical Transitions in Atomically Thin Semiconductors. *Phys. Rev. B* **2018**, *97*, 041409.
(37) Raja, A.; Chaves, A.; Yu, J.; Arefe, G.; Hill, H. M.; Rigosi, A. F.; Berkelbach, T. C.; Nagler, P.; Schüller, C.; Korn, T.; et al. Coulomb Engineering of the Bandgap and Excitons in Two-Dimensional Materials. *Nat. Commun.* **2017**, *8*, 15251.

https://doi.org/10.1021/acs.nanolett.3c02897
Nano Lett. 2023, 23, 9936−9942

(38) Su, H.; Xu, D.; Cheng, S.-W.; Li, B.; Liu, S.; Watanabe, K.; Taniguchi, T.; Berkelbach, T. C.; Hone, J. C.; Delor, M. Dark-Exciton Driven Energy Funneling into Dielectric Inhomogeneities in Two-Dimensional Semiconductors. *Nano Lett.* **2022**, *22*, 2843−2850.
(39) Raja, A.; Waldecker, L.; Zipfel, J.; Cho, Y.; Brem, S.; Ziegler, J. D.; Kulig, M.; Taniguchi, T.; Watanabe, K.; Malic, E.; Heinz, T. F.; Berkelbach, T. C.; Chernikov, A. Dielectric Disorder in Two-Dimensional Materials. *Nat. Nanotechnol.* **2019**, *14*, 832−837.
(40) Xu, Y.; Liu, S.; Rhodes, D. A.; Watanabe, K.; Taniguchi, T.; Hone, J.; Elser, V.; Mak, K. F.; Shan, J. Correlated Insulating States at Fractional Fillings of Moiré Superlattices. *Nature* **2020**, *587*, 214−218.
(41) Jin, C.; Kim, J.; Suh, J.; Shi, Z.; Chen, B.; Fan, X.; Kam, M.; Watanabe, K.; Taniguchi, T.; Tongay, S.; Zettl, A.; Wu, J.; Wang, F. Interlayer Electron-Phonon Coupling in WSe_2/HBN Heterostructures. *Nat. Phys.* **2017**, *13*, 127−131.
(42) Chow, C. M.; Yu, H.; Jones, A. M.; Yan, J.; Mandrus, D. G.; Taniguchi, T.; Watanabe, K.; Yao, W.; Xu, X. Unusual Exciton-Phonon Interactions at van Der Waals Engineered Interfaces. *Nano Lett.* **2017**, *17*, 1194−1199.
(43) Viner, J. J. S.; McDonnell, L. P.; Rivera, P.; Xu, X.; Smith, D. C. Insights into Hyperbolic Phonon Polaritons in HBN Using Raman Scattering from Encapsulated Transition Metal Dichalcogenide Layers. *Phys. Rev. B* **2021**, *104*, 165404.
(44) Du, L.; Zhao, Y.; Jia, Z.; Liao, M.; Wang, Q.; Guo, X.; Shi, Z.; Yang, R.; Watanabe, K.; Taniguchi, T.; Xiang, J.; Shi, D.; Dai, Q.; Sun, Z.; Zhang, G. Strong and Tunable Interlayer Coupling of Infrared-Active Phonons to Excitons in van Der Waals Heterostructures. *Phys. Rev. B* **2019**, *99*, 205410.
(45) Du, L.; Liao, M.; Tang, J.; Zhang, Q.; Yu, H.; Yang, R.; Watanabe, K.; Taniguchi, T.; Shi, D.; Zhang, Q.; Zhang, G. Strongly Enhanced Exciton-Phonon Coupling in Two-Dimensional WSe_2. *Phys. Rev. B* **2018**, *97*, 235145.
(46) Zhao, W.; Ghorannevis, Z.; Amara, K. K.; Pang, J. R.; Toh, M.; Zhang, X.; Kloc, C.; Tan, P. H.; Eda, G. Lattice Dynamics in Mono- and Few-Layer Sheets of WS_2 and WSe_2. *Nanoscale* **2013**, *5*, 9677−9683.
(47) Cuscó, R.; Artús, L.; Edgar, J. H.; Liu, S.; Cassabois, G.; Gil, B. Isotopic Effects on Phonon Anharmonicity in Layered van Der Waals Crystals: Isotopically Pure Hexagonal Boron Nitride. *Phys. Rev. B* **2018**, *97*, 155435.
(48) Gorbachev, R. V.; Riaz, I.; Nair, R. R.; Jalil, R.; Britnell, L.; Belle, B. D.; Hill, E. W.; Novoselov, K. S.; Watanabe, K.; Taniguchi, T.; Geim, A. K.; Blake, P. Hunting for Monolayer Boron Nitride: Optical and Raman Signatures. *Small* **2011**, *7*, 465−468.
(49) Passler, N. C.; Paarmann, A. Generalized 4 × 4 Matrix Formalism for Light Propagation in Anisotropic Stratified Media: Study of Surface Phonon Polaritons in Polar Dielectric Heterostructures: Erratum. *J. Opt. Soc. Am. B* **2019**, *36*, 3246−3248.
(50) Lindfors, K.; Kalkbrenner, T.; Stoller, P.; Sandoghdar, V. Detection and Spectroscopy of Gold Nanoparticles Using Supercontinuum White Light Confocal Microscopy. *Phys. Rev. Lett.* **2004**, *93*, 037401.
(51) Taylor, R. W.; Sandoghdar, V. Interferometric Scattering Microscopy: Seeing Single Nanoparticles and Molecules via Rayleigh Scattering. *Nano Lett.* **2019**, *19*, 4827−4835.
(52) Ortega-Arroyo, J.; Kukura, P. Interferometric Scattering Microscopy (ISCAT): New Frontiers in Ultrafast and Ultrasensitive Optical Microscopy. *Phys. Chem. Chem. Phys.* **2012**, *14*, 15625−15636.
(53) Delor, M.; Weaver, H. L.; Yu, Q.; Ginsberg, N. S. Imaging Material Functionality through Three-Dimensional Nanoscale Tracking of Energy Flow. *Nat. Mater.* **2020**, *19*, 56−62.
(54) Ginsberg, N. S.; Tisdale, W. A. Spatially Resolved Photogenerated Exciton and Charge Transport in Emerging Semiconductors. *Annu. Rev. Phys. Chem.* **2020**, *71*, 1−30.
(55) Zhu, T.; Snaider, J. M.; Yuan, L.; Huang, L. Ultrafast Dynamic Microscopy of Carrier and Exciton Transport. *Annu. Rev. Phys. Chem.* **2019**, *70*, 219−244.
(56) Henry, C. H.; Hopfield, J. J. Raman Scattering by Polaritons. *Phys. Rev. Lett.* **1965**, *15*, 964−966.
(57) Merlin, R. Generating Coherent THz Phonons with Light Pulses. *Solid State Commun.* **1997**, *102*, 207−220.
(58) Crimmins, T. F.; Stoyanov, N. S.; Nelson, K. A. Heterodyned Impulsive Stimulated Raman Scattering of Phonon-Polaritons in LiTaO3 and LiNbO3. *J. Chem. Phys.* **2002**, *117*, 2882−2896.
(59) Feurer, T.; Vaughan, J. C.; Nelson, K. A. Spatiotemporal Coherent Control of Lattice Vibrational Waves. *Science* **2003**, *299*, 374−377.
(60) Bergeron, A.; Gradziel, C.; Leonelli, R.; Francoeur, S. Probing Hyperbolic and Surface Phonon-Polaritons in 2D Materials Using Raman Spectroscopy. *Nat. Commun.* **2023**, *14*, 4098.
(61) Mante, P.-A.; Lehmann, S.; Shapiro, D. F.; Lee, K.; Wallentin, J.; Borgström, M. T.; Yartsev, A. Ultrafast Optical Generation of Coherent Bright and Dark Surface Phonon Polaritons in Nanowires. *ACS Photonics* **2020**, *7*, 1923−1931.
(62) Wahlstrand, J. K.; Merlin, R. Cherenkov Radiation Emitted by Ultrafast Laser Pulses and the Generation of Coherent Polaritons. *Phys. Rev. B* **2003**, *68*, 054301.
(63) Cadiz, F.; Robert, C.; Courtade, E.; Manca, M.; Martinelli, L.; Taniguchi, T.; Watanabe, K.; Amand, T.; Rowe, A. C. H.; Paget, D.; et al. Exciton Diffusion in WSe_2 Monolayers Embedded in a van Der Waals Heterostructure. *Appl. Phys. Lett.* **2018**, *112*, 152106.
(64) Zipfel, J.; Kulig, M.; Perea-Causín, R.; Brem, S.; Ziegler, J. D.; Rosati, R.; Taniguchi, T.; Watanabe, K.; Glazov, M. M.; Malic, E.; Chernikov, A. Exciton Diffusion in Monolayer Semiconductors with Suppressed Disorder. *Phys. Rev. B* **2020**, *101*, 115430.
(65) Yuan, L.; Wang, T.; Zhu, T.; Zhou, M.; Huang, L. Exciton Dynamics, Transport, and Annihilation in Atomically Thin Two-Dimensional Semiconductors. *J. Phys. Chem. Lett.* **2017**, *8*, 3371−3379.
(66) Xu, D.; Mandal, A.; Baxter, J. M.; Cheng, S.-W.; Lee, I.; Su, H.; Liu, S.; Reichman, D. R.; Delor, M. Ultrafast Imaging of Polariton Propagation and Interactions. *Nat. Commun.* **2023**, *14*, 3881.
(67) Xu, H.; Wang, X.; Jiang, X.; Dai, X.; Xiang, Y. Guiding Characteristics of Guided Waves in Slab Waveguide with Hexagonal Boron Nitride. *J. Appl. Phys.* **2017**, *122*, 033103.
(68) Dolado, I.; Alfaro Mozaz, F. J.; Li, P.; Nikulina, E.; Bylinkin, A.; Liu, S.; Edgar, J. H.; Casanova, F.; Hueso, L. E.; Alonso González, P.; et al. Nanoscale Guiding of Infrared Light with Hyperbolic Volume and Surface Polaritons in van Der Waals Material Ribbons. *Adv. Mater.* **2020**, *32*, 1906530.
(69) Cui, Q.; Ceballos, F.; Kumar, N.; Zhao, H. Transient Absorption Microscopy of Monolayer and Bulk WSe_2. *ACS Nano* **2014**, *8*, 2970−2976.
(70) Datta, K.; Lyu, Z.; Li, Z.; Taniguchi, T.; Watanabe, K.; Deotare, P. B. Spatiotemporally Controlled Room-Temperature Exciton Transport under Dynamic Strain. *Nat. Photonics* **2022**, *16*, 242−247.
(71) Lazić, S.; Violante, A.; Cohen, K.; Hey, R.; Rapaport, R.; Santos, P. V. Scalable Interconnections for Remote Indirect Exciton Systems Based on Acoustic Transport. *Phys. Rev. B* **2014**, *89*, 85313.
(72) Rudolph, J.; Hey, R.; Santos, P. V. Long-Range Exciton Transport by Dynamic Strain Fields in a GaAs Quantum Well. *Phys. Rev. Lett.* **2007**, *99*, 047602.
(73) Violante, A.; Cohen, K.; Lazić, S.; Hey, R.; Rapaport, R.; Santos, P. V. Dynamics of Indirect Exciton Transport by Moving Acoustic Fields. *New J. Phys.* **2014**, *16*, 033035.
(74) Peng, R.; Ripin, A.; Ye, Y.; Zhu, J.; Wu, C.; Lee, S.; Li, H.; Taniguchi, T.; Watanabe, K.; Cao, T.; et al. Long-Range Transport of 2D Excitons with Acoustic Waves. *Nat. Commun.* **2022**, *13*, 1334.

https://doi.org/10.1021/acs.nanolett.3c02897
Nano Lett. 2023, 23, 9936−9942